

On the Lateral Entrainment Instability in the Inner Core Region of Tropical Cyclones

Ping Zhu¹, Jun A Zhang², and Frank Marks³

¹Florida International University

²Hurricane Research Division, AOML, NOAA

³NOAA/AOML

December 13, 2022

Abstract

Entrainment of dry moat air with low equivalent potential temperature laterally into the eyewall and rainbands is a unique turbulent process in the inner-core region of a tropical cyclone (TC). By analyzing in-situ aircraft measurements collected by the reconnaissance flights that penetrated the eyewalls and rainbands of Hurricanes Rita (2005), Patricia (2015), Harvey (2017), and Michael (2018), as well as numerical simulations of Hurricanes Patricia (2015) and Michael (2018), we show that the moat air entrained into the eyewall and rainbands meets the instability criterion, and therefore, sinks unstably as a convective downdraft. The resultant positive buoyancy fluxes are an important source for the turbulent kinetic energy (TKE) in the eyewall and rainband clouds. This mechanism of TKE generation via lateral entrainment instability should be included in the TKE-type turbulent mixing schemes for a better representation of turbulent transport processes in numerical forecasts of TCs.

Hosted file

951843_0_art_file_10523633_rm9fj.docx available at <https://authorea.com/users/565837/articles/612711-on-the-lateral-entrainment-instability-in-the-inner-core-region-of-tropical-cyclones>

Hosted file

951843_0_supp_10522329_rmmpzk.docx available at <https://authorea.com/users/565837/articles/612711-on-the-lateral-entrainment-instability-in-the-inner-core-region-of-tropical-cyclones>

1
2 **On the Lateral Entrainment Instability in the Inner Core Region of Tropical**
3 **Cyclones**

4 **Ping Zhu¹, Jun A. Zhang^{2,3}, and Frank D. Marks³**

5 ¹Department of Earth and Environment, Florida International University

6 ²Cooperative Institute for Marine and Atmospheric Studies, University of Miami

7 ³Hurricane Research Division, Atlantic Oceanographic and Meteorological Laboratory, NOAA

8
9 Corresponding author: Ping Zhu (zhup@fiu.edu), 11200 SW 8th ST, Miami, FL, 33199.

10 **Key Points:**

- 11 • Lateral entrainment of air from the moat region into eyewall and rainbands of a tropical
12 cyclone satisfies the instability criterion.
- 13 • Positive buoyancy flux induced by the entrainment is an important source of turbulent
14 kinetic energy for the eyewall and rainband clouds.
- 15 • Lateral entrainment instability should be included in turbulent mixing parameterizations
16 in tropical cyclone forecast models.
17

18 **Abstract**

19 Entrainment of dry moat air with low equivalent potential temperature laterally into the eyewall
20 and rainbands is a unique turbulent process in the inner-core region of a tropical cyclone (TC).
21 By analyzing in-situ aircraft measurements collected by the reconnaissance flights that
22 penetrated the eyewalls and rainbands of Hurricanes Rita (2005), Patricia (2015), Harvey (2017),
23 and Michael (2018), as well as numerical simulations of Hurricanes Patricia (2015) and Michael
24 (2018), we show that the moat air entrained into the eyewall and rainbands meets the instability
25 criterion, and therefore, sinks unstably as a convective downdraft. The resultant positive
26 buoyancy fluxes are an important source for the turbulent kinetic energy (TKE) in the eyewall
27 and rainband clouds. This mechanism of TKE generation via lateral entrainment instability
28 should be included in the TKE-type turbulent mixing schemes for a better representation of
29 turbulent transport processes in numerical forecasts of TCs.

30

31 **Plain Language Summary**

32 Turbulence is commonly regarded as a chaotic flow feature pertaining to the planetary boundary
33 layer (PBL). In the inner core of a tropical cyclone (TC), however, turbulence can also be
34 generated in the eyewall and rainbands above the PBL by cloud processes. The turbulence at the
35 edge of the eyewall/rainbands not only experiences the large lateral thermodynamic contrasts
36 across the interface between clouds and moat but also entrains moat air into clouds. Previous
37 studies suggest that under certain conditions the entrained air into the clouds can sink unstably as
38 convective downdrafts, leading to the generation of turbulent kinetic energy (TKE) in the clouds.
39 By analyzing in-situ aircraft measurements collected during the reconnaissance flights that
40 penetrated the eyewalls and rainbands of Hurricanes Rita (2005), Patricia (2015), Harvey (2017),
41 and Michael (2018), as well as numerical simulations of Patricia (2015) and Michael (2018), this
42 study shows that the moat air entrained into the eyewall and rainbands meets the instability
43 criterion. An estimate of the entrainment buoyancy fluxes suggests that the lateral entrainment
44 instability is an important source of TKE in the eyewall and rainbands, and thus, it needs to be
45 included in the TKE-type turbulence schemes used in numerical forecasts of TCs.

46

47 1 Introduction

48 The entrainment instability at the top of clouds was first recognized by Lilly (1968) and
 49 later well documented by Deardorff (1980) and Randall (1980). Under cloud free conditions,
 50 entrainment of air from the free atmosphere above into the turbulent boundary layer tends to
 51 destroy the turbulent kinetic energy (TKE) since the buoyancy force acts to oppose the vertical
 52 motions in the boundary layer. For the boundary layer topped by stratocumulus clouds, however,
 53 the evaporative cooling of the unsaturated free atmosphere air that has been entrained into clouds
 54 may cause the entrained air to sink unstably as a convective downdraft owing to its negative
 55 buoyancy. This process leads to the generation of TKE in the stratocumulus layer. Deardorff
 56 (1980) showed that the entrainment buoyancy flux, $(\overline{w'\theta'_v})_{ctp,e}$, may be written as a function of
 57 the jumps of conserved thermodynamic variables across the top of the stratocumulus layer as,

$$58 \quad (\overline{w'\theta'_v})_{ctp,e} = w_{ctp,e}(-\alpha\Delta_{ctp}\theta_e + \bar{\theta}\Delta_{ctp}q_t), \quad (1)$$

59 where θ_e is the equivalent potential temperature defined as $\theta_e = \theta(1 + \frac{L}{c_p T}q)$; T is temperature;
 60 θ is potential temperature; q is water vapor mixing ratio; L is specific latent heat of vaporization;
 61 c_p is the specific heat of dry air at the constant pressure; q_t is total water mixing ratio; θ_v is
 62 virtual potential temperature; $w_{ctp,e}$ is the cloud-top entrainment velocity; α is a theoretical
 63 coefficient resulting from the derivation involving with the moist thermodynamics, and it has a
 64 value near 0.5, but may vary from 1/3 to 2/3 depending on specific conditions; Δ_{ctp} is defined as
 65 the difference of the above-cloud value minus the in-cloud value; and overbar and prime indicate
 66 the mean and perturbations away from the mean, respectively. Since $w_{ctp,e}$ is positive and
 67 $\Delta_{ctp}q_t$ is negative, if $\Delta_{ctp}\theta_e$ is more negative than a criterion, $\Delta_{ctp}\theta_e < (\Delta_{ctp}\theta_e)_{crit} =$
 68 $\bar{\theta}\Delta_{ctp}q_t/\alpha$, it will, then, result in positive entrainment buoyancy fluxes, $(\overline{w'\theta'_v})_{ctp,e} > 0$, leading
 69 to the generation of TKE in the stratocumulus layer. This is known as the cloud top entrainment
 70 instability and has been identified as an important mechanism for generating TKE in the clouds
 71 to maintain the stratocumulus layer.

72 Unlike the shallow-cloud topped boundary layer that is cleanly separated from the dry
 73 free atmosphere above by a capping inversion, observations show that in the eyewall and
 74 rainbands of a tropical cyclone (TC) large TKEs extend all the way to the upper troposphere
 75 from the boundary layer (e.g., Marks et al. 2008; Lorsolo et al. 2010, Zhang & Montgomery
 76 2012, and Zhu et al. 2019) with no physical interface, such as an inversion, separating the
 77 turbulence generated by boundary layer processes and cloud processes aloft. Thus, cloud top
 78 entrainment instability associated with the shallow stratocumulus does not exist or is negligible
 79 in the TC inner-core region. However, turbulence generated in the eyewall and rainbands
 80 experiences a large lateral thermodynamic contrast across the interface between the
 81 eyewall/rainbands and moat. As an illustration, Figure 1 shows a height-radius distribution of the
 82 simulated total water mixing ratio and velocity vectors at the outer edge of the eyewall from a
 83 large eddy simulation (LES) of Hurricane Isabel (2003) given by Li et al. (2022). There are two
 84 well-defined large overturning eddy circulations in the scene. One is in the boundary layer and
 85 the other is in the mid troposphere at the cloud edge indicated by the thick black arrows. In both
 86 cases, turbulent eddies not only experience drastic lateral contrasts across the edge of the
 87 eyewall, but also entrain the dry and low θ_e air from the moat region laterally into the eyewall.
 88 Following the entrainment instability requirement (Deardorff 1980), if the lateral entrainment of
 89 the low θ_e moat air into the eyewall or rainbands meets the instability criterion, i.e.,

$$\Delta_{lat}\theta_e < (\Delta_{lat}\theta_e)_{crit} = \bar{\theta}\Delta_{lat}q_t/\alpha, \quad (2)$$

where Δ_{lat} refers to the lateral difference of the moat-air value minus the in-cloud value, then, lateral entrainment instability can occur, resulting in positive lateral entrainment buoyancy fluxes. This positive buoyancy flux can in turn serve as an important source for TKE generation in the eyewall and rainbands via buoyancy production of TKE (Stull 1988).

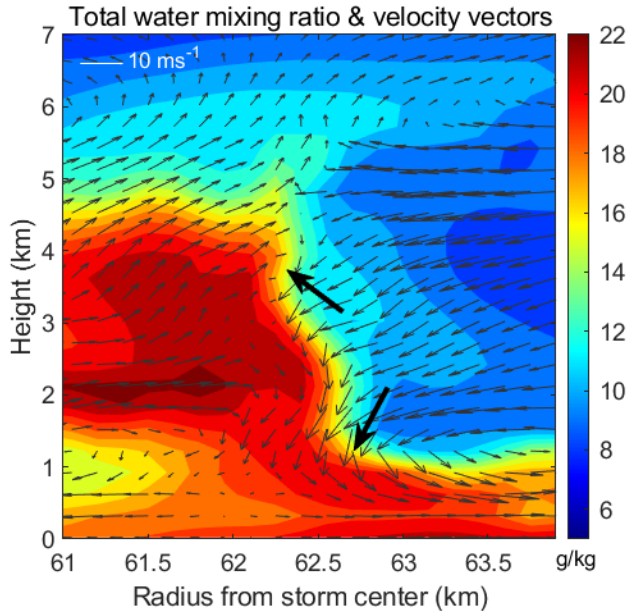


Figure 1: Height-radius distribution of total water mixing ratio (shading, g/kg) overlapped with the wind vectors associated with vertical velocity and radial flow near the outer edge of the eyewall from a large eddy simulation of Hurricane Isabel (2003) documented by Li et al. (2022). To clearly show the overturning eddy circulations, the mean radial flow over the area has been removed. Two thick dark arrows indicate the overturning turbulent eddy circulations in the scene.

111

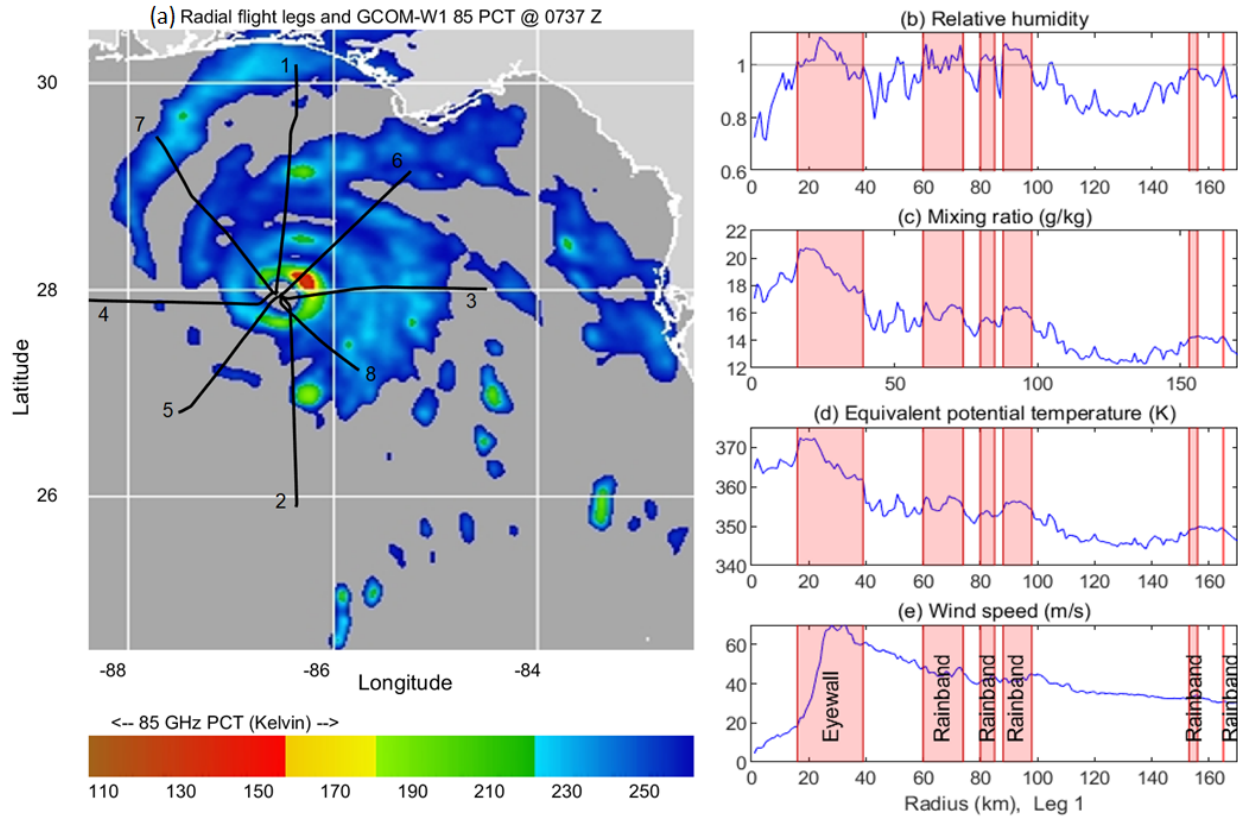
Therefore, the main objective of this study is to verify if the lateral entrainment in the TC inner-core region satisfies the instability criterion stated above using both observations and numerical simulations. The importance and potential application of this TKE generation mechanism in eyewall and rainband clouds via lateral entrainment instability to the TKE type of turbulent mixing parameterizations used in TC forecast models are then discussed.

2 Evidences of lateral entrainment instability in TC inner core

To evaluate if the moat air laterally entrained into the eyewall and rainband clouds meets the instability criterion and is able to sink unstably as a convective downdraft, we examined the in-situ aircraft data collected during the Hurricane Research Division (HRD) reconnaissance flights that penetrated the eyewall and rainbands of Hurricanes Rita (2005), Patricia (2015), Harvey (2017), and Michael (2018) in total 113 radial legs. As an illustration, Figure 2 shows the 8 flight routes into Michael (2018) and the radial profiles of relative humidity, water vapor mixing ratio, equivalent potential temperature θ_e , and wind speed as a function of the distance from the storm center (i.e., radius) at approximately 750 hPa altitude from one of these legs that penetrated into Michael (2018). Details of the radial leg data from the HRD reconnaissance flights are provided in the supporting information file (S1). Since the flights do not have cloud measurements, we infer the locations of eyewall and rainbands as the radii where relative humidities are close to or exceed 1 as shown in Figs. 2b – 2e. We tested several values of relative humidity for saturation from 93% to 97%. It only shows a marginal effect on the analysis results. Therefore, in this paper the eyewall and rainbands in the radial legs are identified wherever the relative humidity exceeds 94%. The eyewall is, then, defined to be the region closest to the

132

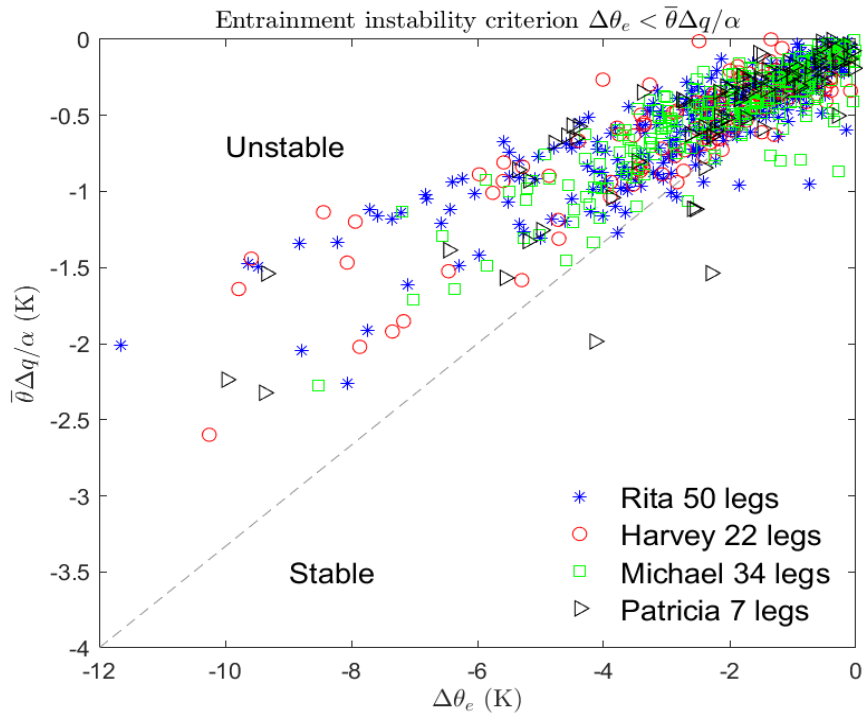
133 maximum wind speed. The radial profile shown in Fig. 2d clearly show that the moat air in-
 134 between eyewall and rainbands has a lower θ_e than the saturated air in the eyewall and
 135 rainbands.



136
 137 *Figure 2: (a): Selected flights that penetrated into the eyewall and rainbands of Hurricane*
 138 *Michael (2018). (b) – (e): Radial profiles of relative humidity, water vapor mixing ratio,*
 139 *equivalent potential temperature, and wind speed as a function of radii from the storm center at*
 140 *~ 750 hPa respectively from one of the flight legs.*

141 We then estimate the difference of θ_e and mixing ratio between the identified unsaturated
 142 moat region and saturated eyewall and rainbands as follows. Since the radial resolution of the
 143 flight data is ~100 – 150 m, we average twenty observation points (~ 2 – 3 km) just inside and
 144 outside of the identified eyewall and rainbands to represent the mean thermodynamic properties
 145 of cloudy and moat air in the lateral entrainment, and then, calculate their differences between
 146 the moat and saturated eyewall and rainbands to examine if the entrained moat air into the
 147 eyewall and rainbands meets the instability criterion. Figure 3 shows the estimated $\Delta\theta_e$ against
 148 the instability criterion $\bar{\theta}\Delta q/\alpha$ for all edges between the identified eyewalls/rainbands and
 149 moats of the 50 radial flight legs into Rita (2005), 7 legs into Patricia (2015), 22 legs into Harvey
 150 (2017), and 34 legs into Michael (2018). Most (>95%) of the estimates fall clearly in the unstable
 151 regime! It should be pointed out that due to the lack of hydrometeor measurements in the aircraft
 152 data we have to replace the total water mixing ratio with the water vapor mixing ratio when
 153 calculating the instability criterion. Therefore, the actual value of $\bar{\theta}\Delta q/\alpha$ should be slightly more
 154 negative if the total water mixing ratio q_t were used. However, even if the hydrometeor mixing
 155 ratios were available and included in the calculation, the majority of the data points should still
 156 fall in the unstable regime, indicating that the moat air that is entrained laterally into eyewall and

157 rainband clouds has sufficiently low θ_e to meet the instability criterion and sinks unstably due to
 158 its own negative buoyancy. It should be noted that the above analysis only shows an entrainment



instability potential. It remains unknown what percentage of moat air is actually entrained into the eyewall and rainband clouds by turbulence. This issue needs to be further investigated using relevant high-resolution observations and LESs.

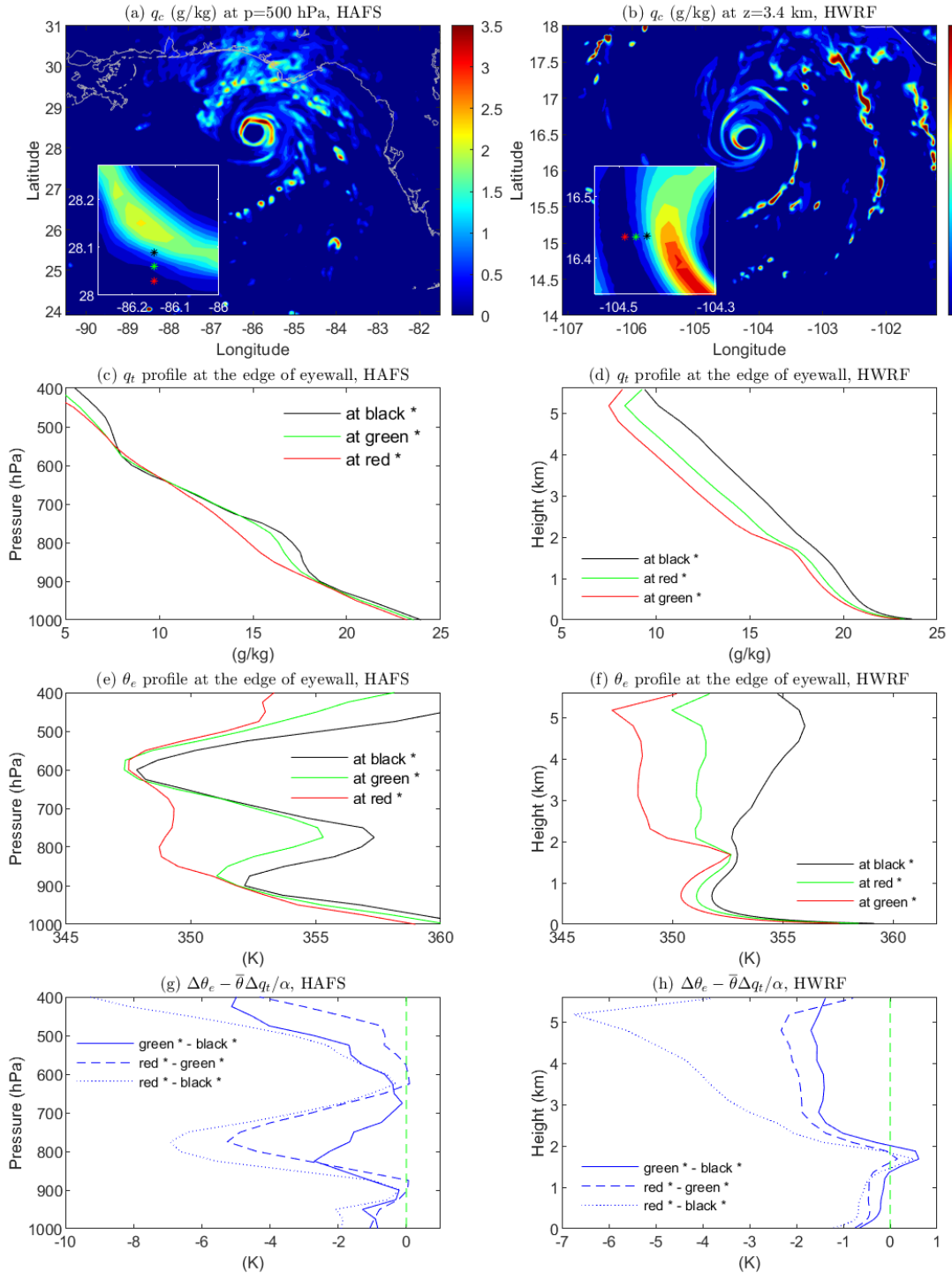
Figure 3: Equivalent potential temperature jumps across the identified eyewall/rainbands and moat, $\Delta\theta_e$, as a function of the corresponding

178 $\bar{\theta}\Delta q/\alpha$ for 50 flight legs into Rita (2005), 7 legs into Patricia (2015), 22 legs into Harvey
 179 (2017), and 34 legs into Michael (2018) where Δ is defined as the difference of moat-air value
 180 minus in-cloud value.

181
 182

183 To further evaluate the lateral entrainment instability in the TC inner core, we examined
 184 the numerical simulations of Hurricane Michael (2018) by the global-nested version of Hurricane
 185 Analysis and Forecast System (HAFS-globalnest, Zhu et al. 2021) and Hurricane Patricia (2015)
 186 by the Hurricane Weather Research and Forecasting (HWRF) model version 3.9a. Details of the
 187 numerical simulations are provided in the Supporting Information (S2). Figure 4 shows two
 188 arbitrary snapshots of the thermodynamic state of the simulated Michael (2018) and Patricia
 189 (2015) during their rapid intensification periods. Three consecutive grid points just inside, at, and
 190 outside of the outer edge of the eyewall are randomly selected whose locations with respect to
 191 the eyewall are shown in Figs. 4a and 4b, respectively. The distance between the grid points is
 192 approximately 1.22 km for HWRF since it was configured at the grid resolution of 0.011 degree,
 193 and 3 km for HAFS. Figures 4c – 4f show the vertical profiles of θ_e and q_t at these three grid
 194 points in the two simulations, respectively. We, then, evaluated the entrainment instability across
 195 the edge of the eyewall by calculating the instability parameter $\Delta_{lat}\theta_e - \bar{\theta}\Delta_{lat}q_t/\alpha$ using
 196 various combinations of the differences between the three grid points: green minus red, red
 197 minus black, and green minus black, respectively. The results (Figs. 4g and 4h) clearly show that
 198 $\Delta\theta_e$ is more negative than the instability criterion throughout the vertical column in both
 199 simulations, indicating that the entrained low θ_e moat air into the eyewall meets the instability
 200 criterion and thus will sink spontaneously due to its own negative buoyancy to generate TKE in

201 the eyewall. Note that we have examined the lateral entrainment instability criterion at various
 202 locations along the edge of eyewall with respect to down/up wind shear. All potential
 203 entrainments consistently meet the thermodynamic instability criterion. However, dynamically it
 204 remains unknown which quadrant of the eyewall with respect to wind shear is preferred for
 205 lateral entrainment, and this issue needs to be further investigated.



207 *Figure 4: (a) and (b): Simulated hydrometeor mixing ratio at the altitude of 500 hPa and 3.4 km*
 208 *at an arbitrary time during the rapid intensification of Michael (2018) by HAFS and Patricia*
 209 *(2015) by HWRF, respectively. The inlaid panel shows the zoom-in view of the eyewall. Red,*
 210 *green, and black stars indicate the grid points in the vicinity of the eyewall to be analyzed. (c)*
 211 *and (f): vertical profiles of q_t and θ_e at the red, green, and black grid points, respectively. (g)*
 212 *and (h): Instability parameter calculated using different jumps between green and black grid*
 213 *points, red and green grid points, and red and black grid points, respectively.*

214 **3 Conclusion and discussion**

215 Airborne radar observations show that large TKEs are generated in the eyewalls and
 216 rainbands by cloud processes aloft (e.g., Marks et al. 2008; Lorsolo et al. 2010, Zhang and
 217 Montgomery 2012, and Zhu et al. 2019). The resultant turbulent transport above the boundary
 218 layer plays an important role in the intensification of TCs (Zhu et al, 2019, 2021). In this study,
 219 by analyzing the in-situ aircraft data collected during the reconnaissance flight that penetrated
 220 the eyewall and rainbands of Hurricanes Rita (2005), Patricia (2015), Harvey (2017), and
 221 Michael (2018), as well as numerical simulations of Michael (2018) by HAFS and Patricia
 222 (2015) by HWRF, we show that the moat air if entrained into the eyewalls and rainbands will
 223 meet the instability criterion, leading to the potential unstable convective downdraft. The
 224 importance of this mechanism of TKE generation in the eyewall and rainbands via lateral
 225 entrainment instability may be inferred from an estimation of the resultant entrainment buoyancy
 226 fluxes. Following Eq. (1), the buoyancy fluxes induced by the lateral entrainment of moat air into
 227 the eyewalls and rainbands may be written as, $\rho c_p v_{lat}(-\alpha \Delta_{lat} \theta_e + \bar{\theta} \Delta_{lat} q_t)$, where ρ is the air
 228 density and v_{lat} is the lateral entrainment velocity. Although to date we have little knowledge on
 229 the lateral entrainment velocity in the TC inner core between the moat and convection, a lateral
 230 entrainment velocity of 0.3 m/s for the entrainment into convective thermals was previously
 231 derived from the comprehensive lidar and aircraft measurements (Crum et al. 1987). Based on
 232 the in-situ aircraft measurements (Fig. 3) and numerical simulations (Figs. 4g and 4 h), it is
 233 reasonable to assume the thermodynamic jump across the edge of eyewall and rainband clouds to
 234 be in a range $-\alpha \Delta_{lat} \theta_e + \bar{\theta} \Delta_{lat} q_t = [1 - 4]K$, further taking $v_{lat} = [0.1 - 0.4]m/s$ based on
 235 the available observations (Crum et al. 1987), then, the entrainment buoyancy fluxes would be in
 236 a range of $[100 - 1600] \frac{W}{m^2}$, suggesting that the lateral entrainment instability should be one of
 237 the important mechanisms for generating TKEs in the eyewall and rainband clouds via TKE
 238 buoyancy production (Stull 1988).

239 The TKE-type turbulent mixing schemes now have been adopted in many research and
 240 operational models used for predicting TCs, such as, the Eddy-Diffusivity-Mass-Flux (EDMF)
 241 TKE scheme (Han and Bretherton 2019) used in the HAFS, a multi-scale Unified Forecast
 242 System (UFS) operational model and data assimilation package capable of providing analyses
 243 and forecasts of the inner core structure of TCs out to 7 days. The TKE schemes are attractive
 244 because they can provide a representation of turbulent transport induced by both the boundary-
 245 layer processes and cloud processes aloft in a unified manner regardless of the boundary layer
 246 height, provided that the buoyancy production, shear production, transport, and dissipation of
 247 TKE in a TKE budget equation can be correctly determined. This feature of a TKE scheme is
 248 particularly important in the TC inner core since the boundary layer becomes ill-defined as air
 249 approaches the eyewall and is pulled up into the active convection (Shapiro 1983; Smith et al.
 250 2008, Smith and Montgomery 2010; Zhang et al. 2011). In the eyewalls and rainbands, buoyancy

251 production is an important source of TKE generation. The result presented in this study indicates
252 that the lateral entrainment instability is an important physical process that needs to be included
253 in the calculation of buoyancy production of TKE in numerical forecasts of TCs. Moreover, the
254 lateral entrainment of moat air into the convective eyewalls and rainbands is a process that links
255 horizontal and vertical turbulent mixing in the TC inner core. The positive lateral entrainment
256 buoyancy flux promotes the TKE generation in the eyewall, which ensue enhances the lateral
257 entrainment instability as more low- θ_e air in the moat is entrained into the eyewall. This positive
258 feedback between the TKE generation in the eyewall clouds and lateral entrainment instability is
259 unique for turbulence development and transport in the TC inner-core region, and thus, it must
260 be represented realistically in numerical models for predicting TCs. We believe that the inclusion
261 of lateral entrainment instability in model turbulent mixing schemes could address some of the
262 issues regarding turbulence parameterization in TC simulations and correct prediction of RI
263 raised by some recent studies (e.g., Lu & Wang 2020; Li & Pu 2021). To appropriately include
264 lateral entrainment process in models, future researches are recommended to focus on
265 investigating the dynamic aspect that determines the actual fraction of the moat air entrained into
266 eyewall and rainbands, quantifying the lateral entrainment velocity using observations and large-
267 eddy simulations, and developing appropriate methods to explicitly include lateral entrainment
268 buoyancy fluxes in the calculation of the buoyancy production of TKE in the TKE-based
269 turbulent mixing schemes.

270

271 **Open Research**

272 Aircraft data, numerical simulation data, and Matlab codes for analyzing data used in this study
273 can be accessed at <http://vortex.ihr.c.fiu.edu/download/Entrainment/>.

274

275 **Acknowledgments**

276 This work is supported by NOAA/HFIP under the Grant NA18NWS4680057, NOAA/JTTI
277 under the Grant NA22OAR4590177, and National Science Foundation under the Grants
278 2211307 and 2211308.

279 **References**

- 280 Crum, T. D., Stull, R. B., & Eloranta, E. W (1987), Coincident Lidar and Aircraft Observations
281 of Entrainment into Thermals and Mixed Layers. *J. Climate App. Meteor.*, 26, 774 – 788.
- 282 Deardorff, J. W. (1980), Cloud top entrainment instability. *J. Atmos. Sci.*, 37, 131-147.
- 283 Li, X., & Pu, Z. (2021). Vertical eddy diffusivity parameterization based on a large-eddy
284 simulation and its impact on prediction of hurricane landfall. *Geophysical Research Letters*,
285 48, e2020GL090703. <https://doi.org/10.1029/2020GL090703>.
- 286 Li, Y. B., Zhu, P., Gao, Z. Q., & Cheung, K (2022), Sensitivity of Large Eddy Simulations of
287 Tropical Cyclone to Sub-Grid Scale Mixing Parameterization. *Atmospheric Research*. 265,
288 105922, <https://doi.org/10.1016/j.atmosres.2021>.
- 289 Lilly, D. K. (1968), Models of cloud-topped mixed layer under a strong inversion. *Quart. J. Roy.*
290 *Meteor. Soc.*, 94, 292 – 837.

- 291 Lorusso, S, Zhang, J. A., Marks, F. D., & Gamache, J. (2010), Estimation and mapping of
292 hurricane turbulent energy using airborne Doppler measurements. *Mon. Wea. Rev.*, 138,
293 3656–3670, <https://doi.org/10.1175/2010MWR3183.1>.
- 294 Lu, X., & Wang, X. G., (2019), Improving hurricane analyses and predictions with TCI, IFEX
295 field campaign observations, and CIMSS AMVs using the advanced hybrid data assimilation
296 system for HWRF. Part I: What is missing to capture the rapid intensification of Hurricane
297 Patricia (2015) when HWRF is already initialized with a more realistic analysis? *Mon. Wea.*
298 *Rev.*, 147 (4), 1351 – 1370.
- 299 Marks, F. D., Black, P. G., Montgomery, M. T., & Burpee, R. W. (2008), Structure of the eye
300 and eyewall of Hurricane Hugo (1989). *Mon. Wea. Rev.*, 136, 1237–1259.
301 <https://doi.org/10.1175/2007MWR2073.1>.
- 302 Randall, D. A. (1980), Conditional instability of the first kind upside down. *J. Atmos. Sci.*, 37,
303 125-130.
- 304 Shapiro, L. (1983), The asymmetric boundary-layer flow under a translating hurricane. *J. Atmos.*
305 *Sci.*, 40, 1984–1998. Smith, R. K, Montgomery, M. T., & Vogl, S. (2008), A critique of
306 Emanuel’s hurricane model and potential intensity theory. *Q. J. R. Meteorol. Soc.*, 134, 551–
307 561.
- 308 Smith, R. K, & Montgomery, M. T. (2010), Hurricane boundary layer theory. *Q. J. R. Meteorol.*
309 *Soc.*, 136, 1665–1670.
- 310 Stull, R. B., (1988), *An introduction to boundary-layer meteorology*. Kluwer: Dordrecht, The
311 Netherlands, 670pp.
- 312 Zhang, J. A., R. F. Rogers, D. S. Nolan, & F. D. Marks, (2011), On the characteristic height
313 scales of the hurricane boundary layer. *Monthly Weather Review*, 139, 2523-
314 2535, <https://doi.org/10.1175/MWR-D-10-05017.1>.
- 315 Zhang, J. A., & Montgomery, M. T. (2012). Observational Estimates of the Horizontal Eddy
316 Diffusivity and Mixing Length in the Low-Level Region of Intense Hurricanes, *Journal of*
317 *the Atmospheric Sciences*, 69(4), 1306-1316. <https://doi.org/10.1175/JAS-D-11-0180.1>
- 318 Zhu, P., Tyner, B., Zhang, J. A., Aligo, E., Gopalakrishnan, S., Marks, F. D., Mehra, A., &
319 Tallapragada, V. (2019), Role of eyewall and rainband in-cloud turbulent mixing in tropical
320 cyclone intensification. *Atmospheric Chemistry and Physics*, 19, 14289–14310,
321 <https://doi.org/10.5194/acp-19-14289-2019>.
- 322 Zhu, P., Hazelton, A., Zhang, Z., Marks, D. F., & Tallapragada, V. (2021). The Role of Eyewall
323 Turbulent Transport in the Pathway to Intensification of Tropical Cyclones. *J. Geophys. Res. -*
324 *Atmospheres*. 126(17), e2021JD034983, <https://doi.org/10.1029/2021JD034983>.
- 325